Journal of Colloid and Interface Science 496 (2017) 456–464

Contents lists available at ScienceDirect

Journal of Colloid and Interface Science

journal homepage: www.elsevier.com/locate/jcis

Regular Article

Fluorescent silica nanoparticles with chemically reactive surface: Controlling spatial distribution in one-step synthesis

María L. Vera [a], Antonela Cánneva [b], Cristián Huck-Iriart [a,c], Felix G. Requejo [a], Mónica C. Gonzalez [a], María L. Dell'Arciprete [a,*], Alejandra Calvo [b,*]

[a] Instituto de Investigaciones Fisicoquímicas Teóricas y Aplicadas, Facultad de Ciencias Exactas (INIFTA), Universidad Nacional de La Plata, CONICET, Casilla de Correo 16, Sucursal 4, 1900 La Plata, Argentina
[b] CONICET, YPF TECNOLOGÍA S. A. (Y-TEC), Av. del Petróleo s/n, entre 129 y 143, Berisso, Buenos Aires 1925, Argentina
[c] Escuela de Ciencia y Tecnología, CONICET, Universidad Nacional de San Martín (UNSAM), Campus Miguelete, 25 de Mayo y Francia, 1650 San Martín, Provincia de Buenos Aires, Argentina

GRAPHICAL ABSTRACT

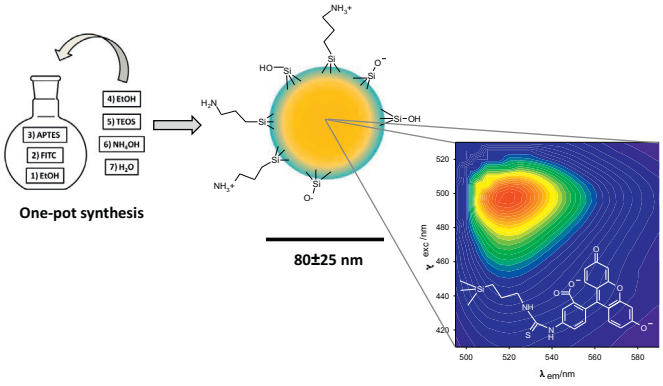

ARTICLE INFO

Article history:
Received 12 December 2016
Revised 14 February 2017
Accepted 15 February 2017
Available online 17 February 2017

Keywords:
Silica nanoparticle
Propylamine surface
Fluorescent nanoparticle
One-pot synthesis

ABSTRACT

The encapsulation of fluorescent dyes inside silica nanoparticles is advantageous to improve their quality as probes. Inside the particle, the fluorophore is protected from the external conditions and its main emission parameters remains unchanged even in the presence of quenchers. On the other hand, the amine-functionalized nanoparticle surface enables a wide range of applications, as amino groups could be easily linked with different biomolecules for targeting purposes. This kind of nanoparticle is regularly synthesized by methods that employ templates, additional nanoparticle formation or multiple pathway process. However, a one-step synthesis will be an efficient approach in this sort of bifunctional hybrid nanoparticles.

A co-condensation sol-gel synthesis of hybrid fluorescent silica nanoparticle where developed. The chemical and morphological characterization of the particles where investigated by DRIFTS, XPS, SEM and SAXS. The nanoparticle fluorescent properties were also assessed by excitation-emission matrices and time resolved experiments.

We have developed a one-pot synthesis method that enables the simultaneous incorporation of functionalities, the fluorescent molecule and the amino group, by controlling co-condensation process. An exhaustive characterization allows the definition of the spatial distribution of the fluorescent probe,

* Corresponding authors.
E-mail addresses: mlauravera@inifta.unlp.edu.ar (M.L. Vera), antonela.canneva@ypftecnologia.com (A. Cánneva), chuck@unsam.edu.ar (C. Huck-Iriart), requejo@fisica.unlp.edu.ar (F.G. Requejo), gonzalez@inifta.unlp.edu.ar (M.C. Gonzalez), mlaura@inifta.unlp.edu.ar (M.L. Dell'Arciprete), alejandra.calvo@ypftecnologia.com (A. Calvo).

http://dx.doi.org/10.1016/j.jcis.2017.02.040

fluorescein isothiocyanate, inside the particle and reactive amino groups on the surface of the nanoparticle with diameter about 100 nm.

1. Introduction

Silica nanoparticles (NP) have attracted wide interest because of their simple preparation, tunable size, optical transparency, high hydrophilicity, biocompatibility, low cytotoxicity and control over particle interactions. Due to these features, NP provides an excellent platform for development of cellular imaging devices and tracking applications [1–3]. Moreover, the richness of the NP surface chemistry opens a wide range of biological applications since can be easily functionalized for further conjugation with antibodies, peptides, DNA, etc. [4–6]. In that sense, the silanes coupling reagents offer broad opportunities and in particular, (3-aminopropyl)triethoxysilane (APTES) is extensively employed [7]. Surface modification is usually done by post-grafting after nanoparticle synthesis to avoid potential secondary nucleation [2] and to provide more accessible functional groups [8]. All synthesis methods described in literature are adaptations of the sol-gel process pioneer by Stöber [9] and employ templates [10–14], additional nanoparticle formation [15] or multiple pathway processes to asses narrow size distribution of NP [16–18].

Fluorescent silica nanoparticles with diameters about 30–130 nm are used as probes for *in vitro* and *in vivo* imaging purposes [11,12,16,19,20]. In these particles the silica matrix serves as a dye isolator limiting the effect of the biological environment on the fluorescent probe [2]. The internalization of these kind of nanomaterials in cells is usually studied by flow cytometry or fluorescent microscopy using different dye-doped nanoparticles containing: rhodamine [21,22], fluorescein isothiocyanate (FITC) [4,23,24] and acridine orange [25–27]. In particular, FITC is a xanthene dye highly soluble in water which presents a high quantum yield, adequate photostability and strong sensitive luminescence to media composition. The dye exists in aqueous environment as cationic, neutral, anionic and dianionic forms [28]. In consequence, its luminescence strongly depends on pH [1,4,29].

To obtain fluorescent NP with amino functionalities on their surface at least two- or three-step synthesis procedure is needed [16,30]. A goal would be to reach a simpler synthesis method, in which fluorophore and external groups are added simultaneously in one-step.

In this work, we developed a one-pot synthesis by adaptation of the Stöber method where all the reactants co-condensate to build hybrid silica nanoparticles [8,4,31], with diameters of about 100 nm without employing a template. Firstly, we designed and characterized propylamino NP by the co-condensation of APTES and TEOS. Secondly, from the previous knowledge, we developed the main scope of this work: APTES and FITC were incorporated in a one-step synthesis controlling the spatial distribution of both functionalities.

2. Experimental section

2.1. Materials

Tetraethyl orthosilicate (TEOS, 98%, Aldrich), (3-aminopropyl) triethoxysilane (APTES, 98%, Aldrich), fluorescein isothiocyanate (FITC, 97.5%, Sigma) ammonia solution (NH_4OH, 28–30%, Aldrich), absolute ethanol (EtOH, 99.5%, Carlo Erba), hydrochloric acid (HCl, 37%, Carlo Erba) and potassium hydroxide (KOH, Anedra) were used without further purification. Deionized water (18 mΩ) was withdrawn from a Millipore instrument.

2.2. Synthesis of propylamine silica nanoparticle

Two synthesis protocols, named as Synthesis A and B were developed to study the amino distribution in the NP by varying the order of reagents addition. A scheme of the experimental procedures is shown at Scheme 1.

For both synthesis procedures 21.2 ml of absolute ethanol, 1.80 ml of TEOS previously mixed with 100 μl of APTES, 0.64 ml of NH_4OH and 1.3 ml of Milli Q grade water were employed. The mixtures were prepared in a 50 ml round-bottomed flask capped with a rubber septum and mixed with under magnetic stirring at 300 rpm for 45 min at 25 °C. In Synthesis A the order of the reactant addition was (1) EtOH, (2) NH_4OH, (3) H_2O and (4) TEOS + APTES; and in Synthesis B (1) EtOH, (2) TEOS + APTES, (3) NH_4OH and (4) H_2O.

The opalescent dispersion obtained in both protocols was washed with absolute ethanol through three cycles of centrifugation (6500 rpm for fifteen minutes)/sonication/redispersion. Solvent was evaporated in an oven at 100 °C for 24 h. Dried powder was kept for further characterization. The obtained product for Synthesis A and B were identified as NPN-A and NPN-B, respectively.

2.3. Synthesis of propylamine fluorescent silica nanoparticle

The experimental procedure is showed in Scheme 2. In a 50 ml round-bottomed flask capped with a rubber septum, 9 ml of absolute ethanol was mixed with 450 μl of FITC (0.021 M in ethanol) and 634 μl APTES. The mixture was magnetically stirred at 300 rpm for 24 h at 25 °C to obtain a FITC-APTES adduct dissolved in the excess of reactant. Then, in the same pot and without any further purification step, all the reagents were added consecutively with an interval of one minute between each other: 12.2 ml of absolute ethanol, 1.8 ml of TEOS, 0.64 ml of NH_4OH and 1.3 ml of Milli-Q grade water. The reaction proceeded for 24 h, without varying the conditions of stirring and temperature. The opalescent orange dispersion was washed with absolute ethanol three times

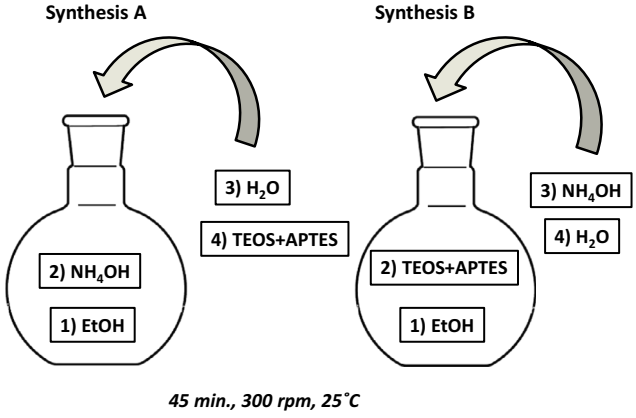

Scheme 1. Schematic illustration of the experimental synthesis procedures A and B used to obtain propylamine silica nanoparticles.

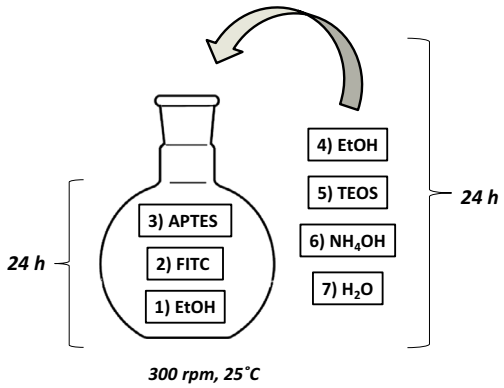

Scheme 2. Schematic illustration of the experimental procedure of the one-pot synthesis of propylamine fluorescent silica nanoparticles.

through cycles of centrifugation (6500 rpm for fifteen minutes)/s onication/redispersion. Solvent was evaporated in an oven at 100 °C for 24 h. Dried powder was storage for further characterization. The obtained sample was identified as NPF.

2.4. Morphological characterization

Small Angle X-ray Scattering (SAXS) experiments were perform at INIFTA facilities using a XEUSS 1.0 equipment from XENOCS with a Kα-Copper radiation microsource (λ = 1.54 Å). A PILATUS-100 K detector was used with 2467 mm sample detector distance. One-dimensional curves were obtained by integration of the 2D data using Foxtrot software. An ethanolic suspension of NP was placed in a liquid sample holder at room temperature. SAXS normalized patterns were fitted using the program McSAS 1.0.1 [32,33]. The software estimate the nanoparticle size distribution function using Monte Carlo simulation by considering spherical particles.

Scanning Electron Microscopy (SEM) measurements were performed at Y-TEC using a FEI QUANTA 200 SEM microscope with an acceleration voltage of 20 kV and a EDT detector. Dried powder samples were supported on a conductive double stick carbon tape.

2.5. Chemical characterization

Diffuse Reflectance Infrared Fourier Transform Spectroscopy (DRIFTS) measurements were carried out using a Nicolet MAGNA 560 instrument at Y-TEC. DRIFTS experiments were performed by depositing dry powdered samples on KBr filled cone sample holder. Spectra were achieved through 64 scans and resolution of 4 cm^{-1}.

X-ray Photoelectron Spectroscopy (XPS) analysis was performed with a SPECS instrument located at Y-TEC Company. Spectra were acquired using a monochromatic AlKα (1486.6 eV), a spectrometer equipped with a dual anode Al/Ag X-ray source and a hemispherical electron energy analyzer. Binding energies are referred to the adventitious C 1s emission at 285 eV. Measurements were carried out on dry powdered samples using a conducting double stick carbon tape. From the integrated intensities of N 1s core levels, quantitative analyses were carried out.

2.6. Fluorescence characterization

Room temperature luminescence measurements were performed with a Jobin-Yvon Spex Fluorolog FL3-11 Spectrometer at INIFTA, which is equipped with a Xe lamp as the excitation source, a monochromator with 1 nm bandpass gap for selecting the excitation and emission wavelengths, and a red sensitive R928 PM detector. The spectra were corrected for the wavelength-dependent sensitivity of the detector and the source. Furthermore, emission spectra were corrected for Raman scattering by using the solvent emission spectrum. Absorbances bellow 0.05 at excitation wavelengths were selected for all samples.

Time resolved photoluminescence measurements were performed with Jobin-Yvon Spex Fluorolog FL3-11 spectrometer (*vide supra*) equipped with TCSPC (time correlated single photon counting) with LED excitation at 461 nm and emission were collected at 520 nm. Decays were recorded until 5000 counts for all samples. Signal deconvolution was performed with DAS 6.5 HORIBA JobinYvon software until optimal values of χ^2.

A bilinear regression analysis taking advantage of the linearity of the intensity of the emission wavelength ($I(\lambda_m)$) with both, the absorption coefficient of the fluorophore at a given excitation wavelength ($\varepsilon(\lambda_x)$) and the factor $F(\lambda_m)$ was applied to the experimental emission matrix. The $F(\lambda_m)$ factor reflects the distribution of the probability of the various transitions from the lowest vibrational level of the first electronic excited level to the various vibrational levels of the ground state. The analysis recovers information on the minimum number of species and on their relative emission and absorption spectra [34].

3. Results and discussion

To build silica nanoparticles with two functionalities in only one-step synthesis is necessary a careful control of the co-condensation precursors during the sol-gel process [35]. Particularly, the incorporation of APTES and FITC (covalently bonded), which are size and chemically strongly different, must be cautiously managed. Otherwise, a non-nanostructured product or a double population of particles could be obtained [36,37].

In this context, we firstly investigated the synthesis of propylamino silica nanoparticle, without fluorophore, which involved only the co-condensation of APTES and the silica precursor (TEOS). Subsequently, we studied the synthesis of propylamine fluorescent silica nanoparticle adding the FITC reactant to the previous developed synthesis.

3.1. Synthesis of propylamine silica nanoparticle

As it was described in Section 2, Synthesis A and B were performed to obtained propylamine silica NP by the co-condensation method [4,31], which are labeled NPN-A and NPN-B, respectively. These protocols were designed to investigate the changes in propylamine groups distribution in the NP volume and surface. Between both procedures only the order of reagents addition was modified, but quantities of all the reactants remain constant.

Fig. 1 shows the morphology by SEM and size distribution achieved by SAXS of the NPN-A and NPN-B. As both samples were easily dispersed in ethanol, a good colloidal stability is proved. Spherical nanoparticles with an average diameter about 110 ± 40 nm were obtained from both syntheses. In Synthesis A, the alkoxides are added to a solution containing the catalyst and the initiator. On the other hand, in Synthesis B, alkoxides are previously diluted with ethanol and then the catalyst and the initiator are added (see Scheme 1). Due to the order of reactants addition, it is expected that a higher local concentration of silanes in Synthesis A, result in larger size nanoparticles. However, a meaningless difference was observed between the histograms.

It is interesting to note that hybrid silica nanoparticles with diameters below 200 nm are hardly obtained without templates [10,11,38] or multiple stage processes [29]. As the reactant order

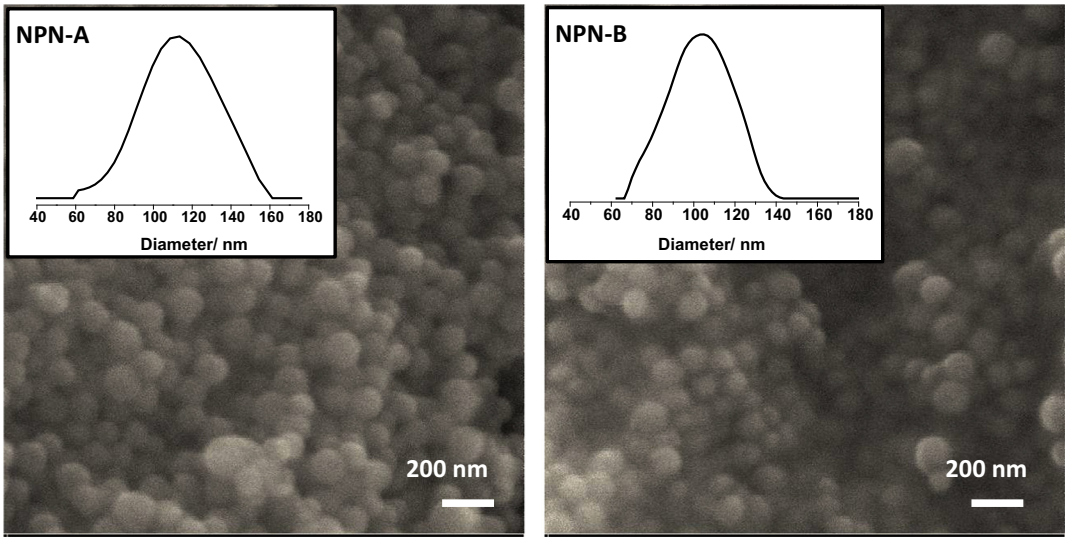

Fig. 1. SEM images of NPN-A (left) and NPN-B (right). Input: size distribution histograms of NP obtained by SAXS.

addition have not a dominant effect in product morphology, the total molar ratios seems to be the key factor in size control.

For a chemical characterization of the NP, DRIFTS and XPS analysis were performed. The results clearly showed the presence of propylamine for both syntheses, as it will be shown below. In order to evaluate the propylamine groups spatial distribution in the nanoparticle volume, we performed a specific experiment as follows [8,39]. The samples were dispersed in aqueous solution at pH 2 and pH 8, and then dried. These pHs values were chosen to achieve the protonation/deprotonation of amino groups without affecting the integrity of the silica matrix. Both species, $-NH_2$ and $-NH_3^+$, show singular signals by DRIFTS and XPS, so they can be distinguished by these techniques. It is expected that only the functionalities on the outside of the nanoparticle is altered by de pH media. As a consequence, by following the variation of $[-NH_2]$ and $[-NH_3^+]$, it is possible to infer the location of the propylamino groups (inside or on the NP surface). Functional groups that were not able to be protonated/deprotonated are isolated inside the silica matrix; in contrast groups that were altered by the media are on the surface.

DRIFTS spectra of NPN-A and NPN-B obtained at both pHs values are shown in Fig. 2. The hybrid samples depict three bands between 1400 and 1750 cm^{-1}. The absorption bands δ_{O-H} at 1650 cm^{-1} result independent of pH and correspond to the O—H vibration, which is the fingerprint of the silica materials. Two bands are observed corresponding to the stretching vibration of δ_{N-H} at 1460–1540 cm^{-1} region. The lower and higher wavenumber bands are attributed to $-NH_2$ and $-NH_3^+$, respectively [39]. For both syntheses, the bands are sensitive to pH, which implies that at least certain amount of propylamino groups is accessible for the medium. However, for NPN-A, larger changes are observed in absorption intensities. At pH 8, the $-NH_2$ band is higher than the $-NH_3^+$ band, and the opposite behavior is observed at pH 2. The result suggested a different propylamino group distribution between both synthesis protocols. A more sensitive technique is necessary to asses a quantitative analysis.

XPS technique was selected for a quantitative evaluation of propylamino group percentage that are encapsulated or accessible to the medium. Although XPS is a surface technique, due to low expected density of hybrid silica materials, the analysis depth is about 10 nm [39]. Taking into account a NP diameter about 100 nm and the analysis depth, the measurements are sensing almost 50% of the total particle volume.

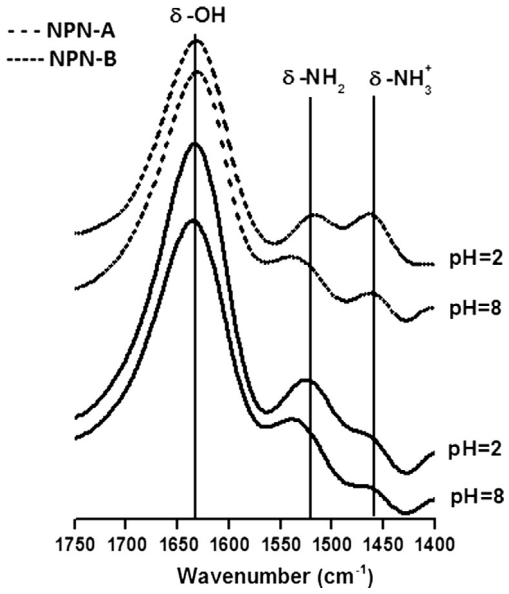

Fig. 2. DRIFTS spectra from NPN-A (dash line spectrum) and NPN-B (full line spectrum) at pH 2 and pH 8.

From the deconvolution of characteristic N1s spectrum of propylamino group in the 397–407 eV region it is possible to calculate the number of $-NH_3^+$ ($n_{-NH_3^+}$) and the total amino content ($n_t = n_{-NH_3^+} + n_{-NH_2}$) at pH 2 and pH 8, see Supporting Information Fig. SI 1. Considering that propylamino group acid-base equilibrium in silica environments differs from the behavior in solution, it is not possible to assume a pK_a value in these hybrid materials. However, as was shown in literature, Eq. (1) allows a low limit estimation of the reachable propylamino groups in the pH range studied in which the nanoparticle integrity is unaffected [39].

$$\%\ \text{reachable propylamino} = \left[\left(\frac{n_{-NH_3^+}}{n_t}\right)_{pH=2} - \left(\frac{n_{-NH_3^+}}{n_t}\right)_{pH=8}\right] \times 100 \quad (1)$$

The percentages of reachable propylamino groups for both samples are shown in Table 1. The data depict that both samples

Table 1
Percentage of reachable amino groups from XPS data, for NPN-A and NPN-B.

Sample	$\frac{n_{-NH_3^+}}{n_t}$	% reachable propylamino
NPN-A, pH 2	0.68	35%
NPN-A, pH 8	0.33	
NPN-B, pH 2	0.52	11%
NPN-B, pH 8	0.41	

present a diverse propylamino groups distribution inside and outside the analysis depth of the NP (~10 nm). A 35% of reachable propylamino groups were obtained for NPN-A in contrast with 11% found for NPN-B. It means that 65% and 89% of propylamino groups are not accessible to the medium, for samples NPN-A and NPN-B, respectively. Thus, although the morphology of NPN-A and NPN-B samples is similar, the concentration of surface propylamino groups is highly dependent on the reactant addition order. As the propylamino groups are excellent linking sites for several molecules, depending on the desired nanoparticle functionalization design one of the above synthesis protocols could be chosen.

3.2. Synthesis of propylamine fluorescent silica nanoparticles

The goal of the present work is to isolate the FITC fluorophore from the external media inside the NP and simultaneously anchor propylamino groups on the surface in just one-pot. The APTES reactant fulfils a double purpose as: fluorophore linker by adduct formation (see Scheme 3) and propylamino group supplier for further functionalization. Previously studied protocols A and B provided surface and encapsulated propylamino groups. Due to the order of reactant addition, Synthesis protocol B is suitable for APTES/FITC adduct incorporation and particles growth in a one-pot procedure.

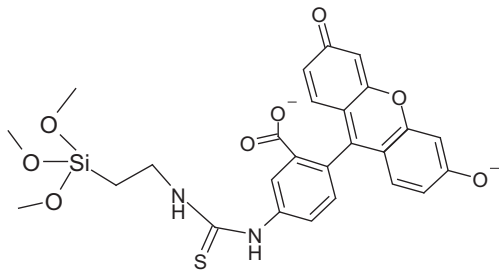

Scheme 3. APTES-FITC adduct structure.

A wide range of APTES/FITC ratios have been reported in the literature for the formation of the adduct [40]. An excess of APTES relative to FITC is needed to complete adduct formation. The ratio used here for the incorporation of FITC to NP was APTES/FITC > 300, with APTES representing the 25% of total alkoxide. The used value is ten times higher than that used for NPN-B synthesis.

The obtained fluorescent silica nanoparticles (NPF) were characterized by SEM, SAXS and DRIFTS to study the morphology, size distribution and chemical functionalization, respectively. Results are shown in Fig. 3. As was mentioned above, the dispersion of NPF sample implies a good colloidal stability. Spherical nanoparticles with an average diameter of 80 ± 25 nm were obtained. That implies a slight decrease in size distribution in comparison with NPN-B sample. The difference could be attributed to the excess of APTES that behaved as an extra amount of catalyst.

To study the chemical functionalization of the nanoparticles, DRIFTS characterization was developed following the same experiment protocol described above. The signals at 1580 and 1540 cm^{-1} assigned to asymmetric bending of $—NH_3^+$ and $—NH_2$ respectively can be distinguished in Fig. 3(b) [41]. Not a meaningful displacement of these signals as a function of the pH was observed. Although the stretching signal —N—H of the APTES-FITC adduct is also expected to be at these energies, no contributions could be distinguished due to the low dye concentration (APTES/FITC > 300). These results prove the presence of propylamine groups in the NPF sample; however no information of the fluorophore was obtained.

Fig. 4 depicts the XPS analysis of NPF at pH 2 (black) and pH 8 (red). The sample was treated following the same experiment protocol described for DRIFTS measurements. The N1s spectra (Fig. 4A) show a noticeable difference between both pH conditions. A broader peak in the 397–407 eV region is observed for pH 2 than for pH 8, which could be attributed to a significant change in the ratio $—NH_3^+/—NH_2$ due to surface protonation. This behavior evidenced the presence of external propylamino groups in the nanoparticle surface. However, as we discussed for NPN-A and NPN-B samples, it is expected that a significant percentage of propylamino groups remains encapsulated inside the NPF.

On the other hand, XPS fingerprint for the FITC has two characteristic signals of N1s and S2s. Nevertheless, as was discussed for

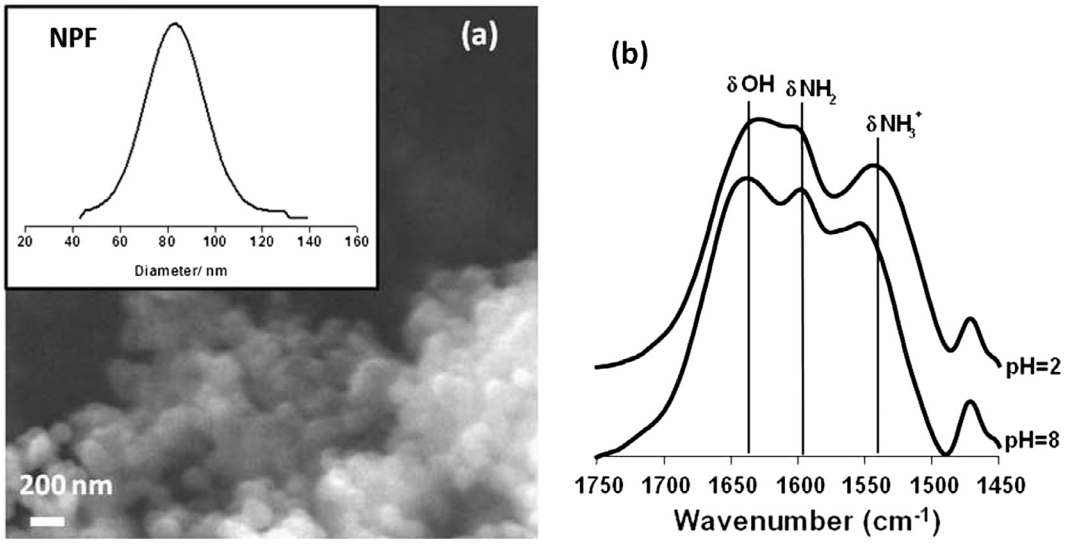

Fig. 3. (a) SEM images of NPF sample. *Input*. Size distribution histogram obtained by SAXS. (b) DRIFTS spectra for NPF at pH 2 and pH 8.

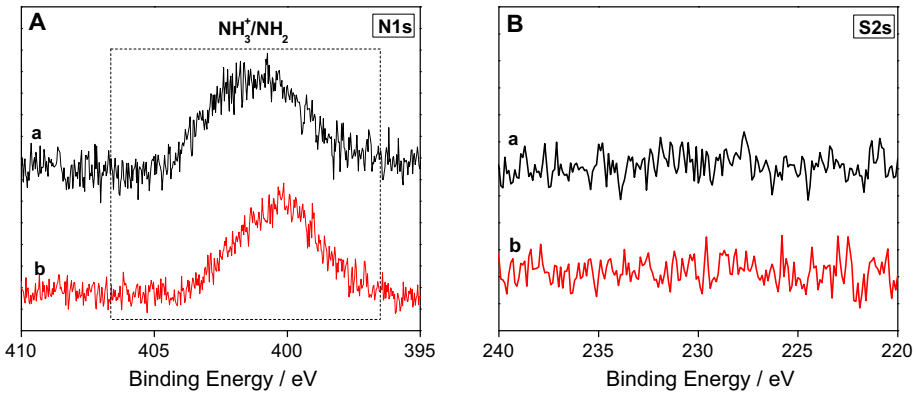

Fig. 4. XPS N1s (A) and S2s (B) spectra of NPF at pH 2 (a) and pH 8 (b).

previous DRIFTS experiments, the low FITC concentration and the overlapping with APTES N1s signals, hinders the dye detection. No peaks were observed in the S2s region for thiourea group at 226.6 eV [42] (Fig. 4B) for both pH conditions. This result supported the observation that no fluorophore moieties are present in the nanoparticle surface neither within 10 nm-depth of the particle volume.

3.3. Fluorescence characterization

The propylamine external functionalization of NPF was demonstrated by chemical characterization analysis. In order to evidence the FITC incorporation, fluorescence characterization techniques were employed.

Several photophysical studies of FITC incorporation on silica nanoparticles are reported in the literature [4,29,43–47]. However, a comprehensive study of the effect of the surrounding environment on the fluorophore optical properties has not been reported. To that purpose, the effect of pH on the optical properties of the encapsulated fluorophore was compared to that observed for free FITC in solution. Therefore, photophysical experiments were performed in aqueous solutions of pH 2 and 8, to monitor different acid-base species of the dye [21,28,30].

3.3.1. Steady state fluorescence spectra of FITC and NPF

Excitation-emission matrix (EEM) of FITC aqueous solution at pH 8 shows fluorescence emission in the wavelength range from 500 to 550 nm, and excitation wavelength in the 450–510 nm range (Fig. 5a). The bilinear regression analysis (Fig. 5c, black lines) of this EEM supports the contribution of one emitting specie with excitation – emission maxima (λ_{exc}/nm, λ_{em}/nm) at (495, 515), in agreement with reported values for the FITC dianionic form [48]. Remarkable differences can be observed in experiments at pH 2. The EEM present a broad emission in the range 490–600 nm and excitation in the wavelength range 400–500 nm (Fig. 5b). The bilinear regression analysis retrieve the presence of one

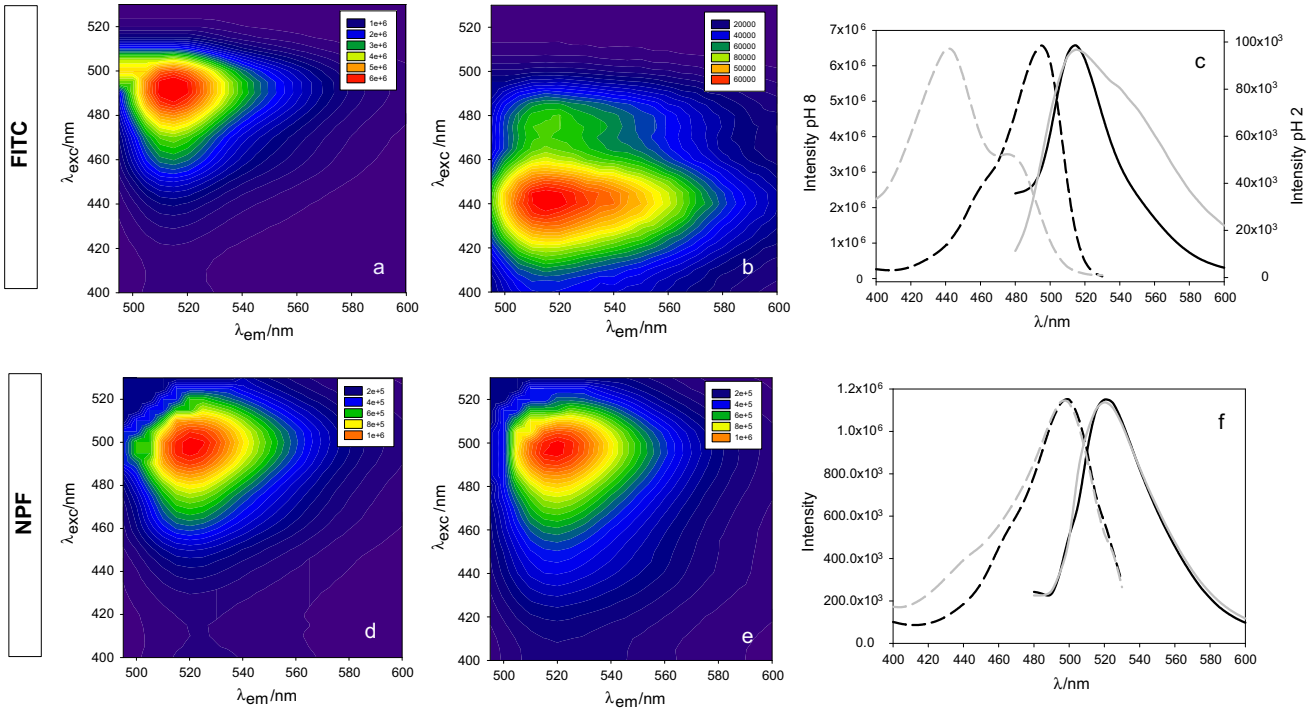

Fig. 5. Top graphs: EEM of an aqueous solution of FITC at pH 8 (a) and pH 2 (b). (c) Emission (full lines) and excitation (dashed lines) of contributing species at pH 8 (black lines) and pH 2 (grey lines). **Bottom graphs**: EEM of aqueous solution of NPF at pH 8 (d) and (e) pH 2. (f) Emission (full lines) and excitation (dashed lines) of contributing species at pH 8 (black lines) and pH 2 (grey lines).

Table 2
Luminescence decay times, and contribution to the total emission, τ (%), obtained upon 461 nm excitation in experiments at 296 K in aqueous solvent for FITC and NPF at pH 2 and pH 8.

Sample	τ_1(ns)	τ_2(ns)
FITC pH 8	3.95 ± 0.01(100%)	–
FITC pH 2	2.21 ± 0.02(56%)	1.16 ± 0.05(44%)
NPF pH 8	3.4 ± 0.1(75%)	1.1 ± 0.1(25%)
NPF pH 2	3.2 ± 0.1(74%)	1.4 ± 0.2(26%)

contributing specie with excitation maxima at 440 and 475 nm, a broad emission with maximum at 515 nm, and shoulder at 545 nm (Fig. 5c, grey lines). The spectra resemble that found in the literature for the anionic form. The excitation of cationic and neutral forms, both contributing at pH 2, leads to the generation of a monoanion excited state with emission maximum at 515 nm and a broad shoulder around 550 nm [28,44]. However, as the neutral form of the dye is present the aggregation of FITC molecules at pH 2 can be discarded [49]. It is worth to note that the ratio of emission intensity at λ_{max} 515 nm for suspensions at pH 8 and pH 2 is $I_{(pH\ 8)}/I_{(pH\ 2)} > 70$.

Coincident EEM were obtained for NPF suspended in aqueous solution at pH 8 and pH 2 (Fig. 5d and e, respectively). The bilinear regression analysis in both conditions presents similar excitation and emission maxima at (λ_{exc}/nm, λ_{em}/nm) at (500, 520) (Fig. 5f). A detailed bilinear regression analysis shows that the maxima are 5 nm shifted to higher wavelengths compared with FITC at pH 8 in aqueous solution and may be attributed to the incorporation of FITC and its interaction with the silica matrix [50,51]. Moreover, the intensity ratio at emission maximum is $I_{(pH\ 8)}/I_{(pH\ 2)} \cong 1$, unlike free FITC behavior. The analysis for NPF suspensions at pH 2 shows a small shoulder at 440 nm excitation in coincidence with the excitation maxima of free FITC at pH 2. Altogether, these observations strongly suggest that most of the incorporated fluorophore is confined in the particle interior as it is protected from changes in the media while a minor fraction is capable of sensing the pH of the media. These observations are in agreement with XPS results showing no contribution to the obtained signals of the fluorophore on the particles surface and in the ~10 nm outer part of the particles.

3.3.2. Time resolved fluorescence emission of FITC and NPF

The fluorescence lifetimes of FITC and NPF were obtained and are detailed in Table 2. The fluorescence decay of FITC aqueous solutions at pH 8 is well fitted with a monoexponential component with fluorescence lifetime $\tau_1 = 3.95$ ns, in good agreement with literature reports for the dianionic emission in aqueous solutions [28,44,45]. At pH 2 FITC solution decay can be well fitted by two exponential with $\tau_1 = 2.21$ ns (56% contribution) and $\tau_2 = 1.16$ ns (44% contribution). The decrease of FITC lifetime in acidic conditions was observed by Liu ($\tau_1 \cong 2.4$ ns at pH 2.3) and Sjöback et al. ($\tau_1 \cong$ 3 ns at pH 3.17) [28,48] though these authors found a single exponential decay attributed to the emission process of the anionic species [28]. According to pK_a values, at pH 2 the FITC cation and neutral forms are present. The short lifetime observed in our experiments could be associated to aggregate formation.

NPF suspension at pH 2 and pH 8 yields luminescence decays that could be fitted considering three contributions. The shortest lifetime of fractions of ns was attributed to scattering and consequently the lifetimes reported yield information on the fluorophore localization. Values of $\tau_1 = 3.4$ ns (75%, contribution neglecting scattering) and $\tau_2 = 1.1$ ns (25%) were obtained at pH 8 while $\tau_1 = 3.2$ ns (74%, contribution neglecting scattering)) and $\tau_2 = 1.4$ ns (26%) were obtained at pH 2. The excellent coincidence between τ_1 and τ_2 values and% of contribution obtained at pH 2 and pH 8 further supports our previous suggestion that the fluorophore molecule is confined in the particle interior. Lifetimes τ_1 and τ_2 might be sensing different environments inside the nanoparticle. Values of $\tau_1 = 3.2$–3.4 ns (74–75% contribution) are in agreement with that observed for FITC incorporated in porous silica at pH 7.93 and 3.48 [44] and might be related to the emission of a dianion form of the fluorophore stabilized by the high concentration of internal propylamino groups. The latter suggestion is also supported by the observed fluorescence spectra of NPF suspensions, *vide supra*. Lifetimes of $\tau_2 = 1.1$–1.4 (25–26% contribution) were attributed in the literature to FITC molecules retained in a non-solvated microenvironment interacting with silanols groups [31,45]. Therefore, NPF lifetimes are mainly sensing two distinct environments inside the nanoparticle: one richer in silanols and the other in amino groups.

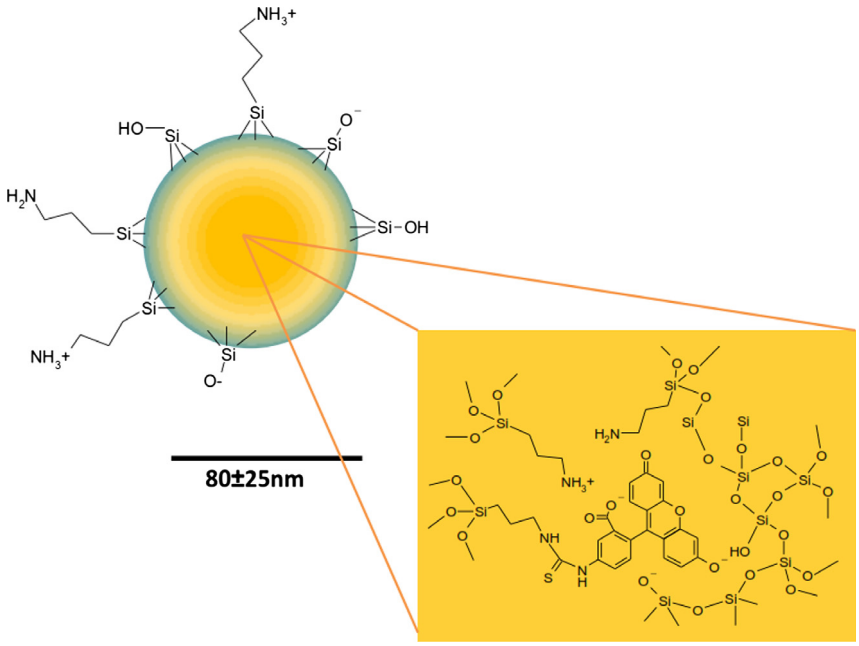

Scheme 4. Schematic representation of NPF.

The contribution of emitting species sensing different environment inside the silica matrix is demonstrated. Moreover, since no changes in lifetimes were observed at both pHs, the encapsulation of a considerable part of the fluorophore is proposed, in agreement with the steady state fluorescence and XPS results.

4. Conclusions

The development of propylamino silica nanoparticles (NPN-A and NPN-B) involving only the co-condensation of APTES and TEOS was effectively reached. The synthesis procedure demonstrated to be robust, as the morphology and size of the product (d = 110 ± 40 nm) is not affected by the order of reactant addition. Moreover, the ratio of surface and encapsulated propylamino groups could be easily tuned, choosing one of these protocols.

With this previous knowledge, fluorescent, propylamine-functionalized silica nanoparticle (NPF) was successfully synthesized by one-pot protocol. Comprehensive characterization of NPF by SEM, SAXS, DRIFTS, XPS and fluorescence techniques demonstrated the yield of spherical nanostructures of diameters of 80 ± 25 nm with amine groups on their surface and FITC confined in the particle interior. The exhaustive analysis of the data allows us to establish the spatial distribution of propylamino and FITC functionalities in the particles, as it is shown in Scheme 4.

The synthesis protocol is easy, affordable, without in-between separation steps, develops at room temperature, without controlling the atmosphere and uses ethanol as solvent. The encapsulated FITC emission maximum position is similar to free FITC although the encapsulation procedure involved the formation of alkoxysilane adduct. The NPF structure demonstrated to protect the dye from external conditions, such as pH. The incorporation of surface amino groups, by co-condensation was also confirmed opening new opportunities for functionalization, as it can be easily conjugated with a wide variety of molecules. The mild reaction conditions offer a promising protocol to encapsulate temperature-sensitive drugs like fluorophores or biomolecules which can be functionalized through APTES. Our work presents a novel contribution in one-step synthesis of emitting silica nanoparticles with reactive surface group with high potential as bioimaging devices and drug nanovehicles.

Acknowledgments

M.L.D, M.C.G., A. C. and F.G.R. are research members of CONICET, Argentina. This research was supported by the grant PICT 2012-2359 and FONARSEC-Nanotecnología 2012/01 from ANPCyT, and by YFP Tecnología S. A. SAXS experiments at INIFTA were performed thanks to project "Nanopymes" (EuropeAid/132184/D/SUP/AR-Contract31-896). The authors thank Maria Alejandra Floridia Addato for SEM images.

Appendix A. Supplementary material

Supplementary data associated with this article can be found, in the online version, at http://dx.doi.org/10.1016/j.jcis.2017.02.040.

References

[1] A. Burns, H. Ow, U. Wiesner, Fluorescent core-shell silica nanoparticles: towards "Lab on a Particle" architectures for nanobiotechnology, Chem Soc Rev. 35 (2006), http://dx.doi.org/10.1039/b600562b.
[2] L. Wang, K. Wang, S. Santra, X. Zhao, L.R. Hilliard, J.E. Smith, Y. Wu, W. Tan, Watching silica nanoparticles glow in the biological world, Anal. Chem. 78 (2006) 646–654, http://dx.doi.org/10.1021/ac0693619.
[3] G. Yao, L. Wang, Y. Wu, J. Smith, J. Xu, W. Zhao, E. Lee, W. Tan, FloDots: luminescent nanoparticles, Anal. Bioanal. Chem. 385 (2006) 518–524, http://dx.doi.org/10.1007/s00216-006-0452-z.
[4] Y. Kotsuchibashi, Y. Zhang, M. Ahmed, M. Ebara, T. Aoyagi, R. Narain, Fabrication of FITC-doped silica nanoparticles and study of their cellular uptake in the presence of lectins, J. Biomed. Mater. Res. Part A 101A (2013) 2090–2096, http://dx.doi.org/10.1002/jbm.a.34498.
[5] W.-H. Zhang, X.-X. Hu, X.-B. Zhang, Dye-doped fluorescent silica nanoparticles for live cell and in vivo bioimaging, Nanomaterials 6 (2016) 81, http://dx.doi.org/10.3390/nano6050081.
[6] C.S. Neves, C.M. Granadeiro, L. Cunha-Silva, D. Ananias, S. Gago, G. Feio, P.A. Carvalho, P. Eaton, S.S. Balula, E. Pereira, Europium polyoxometalates encapsulated in silica nanoparticles – characterization and photoluminescence studies, Eur. J. Inorg. Chem. 2013 (2013) 2877–2886, http://dx.doi.org/10.1002/ejic.201201482.
[7] N.S.K. Gunda, M. Singh, L. Norman, K. Kaur, S.K. Mitra, Optimization and characterization of biomolecule immobilization on silicon substrates using (3-aminopropyl)triethoxysilane (APTES) and glutaraldehyde linker, Appl. Surf. Sci. 305 (2014) 522–530, http://dx.doi.org/10.1016/j.apsusc.2014.03.130.
[8] A. Calvo, M. Joselevich, G.J.A.A. Soler-Illia, F.J. Williams, Chemical reactivity of amino-functionalized mesoporous silica thin films obtained by co-condensation and post-grafting routes, Microporous Mesoporous Mater. 121 (2009) 67–72, http://dx.doi.org/10.1016/j.micromeso.2009.01.005.
[9] W. Stöber, A. Filnk, Controlled growth of monodisperse silica spheres in the micron size range, J. Colloid Interface Sci. 26 (1968), http://dx.doi.org/10.1016/0021-9797(68)90272-5.
[10] R. Lindberg, J. Sjöblom, G. Sundholm, Preparation of silica particles utilizing the sol-gel and the emulsion-gel processes, Colloids Surfaces A Physicochem. Eng. Asp. 99 (1995) 79–88, http://dx.doi.org/10.1016/0927-7757(95)03117-V.
[11] S. Santra, Fluorescent silica nanoparticles for cancer imaging, in: R.S. Grobmyer, M.B. Moudgil (Eds.), Cancer Nanotechnol. Methods Protoc., Humana Press, Totowa, NJ, 2010, pp. 151–162, http://dx.doi.org/10.1007/978-1-60761-609-2_10.
[12] S. Veeranarayanan, A. Cheruvathoor Poulose, S. Mohamed, A. Aravind, Y. Nagaoka, Y. Yoshida, T. Maekawa, D.S. Kumar, FITC labeled silica nanoparticles as efficient cell tags: uptake and photostability study in endothelial cells, J. Fluoresc. 22 (2012) 537–548, http://dx.doi.org/10.1007/s10895-011-0991-3.
[13] M. Darbandi, G. Urban, M. Krüger, Journal of colloid and interface science bright luminescent, colloidal stable silica coated CdSe/ZnS nanocomposite by an in situ, one-pot surface functionalization, J. Colloid Interface Sci. 365 (2012) 41–45, http://dx.doi.org/10.1016/j.jcis.2011.09.024.
[14] M. Darbandi, S. Laurent, M. Busch, Blocked-micropores, surface functionalized, bio-compatible and silica-coated iron oxide nanocomposites as advanced MRI contrast agent, J. Nanopart Res. 15 (2013) 1664–1672, http://dx.doi.org/10.1007/s11051-013-1664-8.
[15] O.V. Makarova, A.E. Ostafin, H. Miyoshi, J.R. Norris, D. Meisel, Adsorption and encapsulation of fluorescent probes in nanoparticles, J. Phys. Chem. B 103 (1999) 9080–9084, http://dx.doi.org/10.1021/jp9900786.
[16] C. Rosu, A.J. Gorman, R. Cueto, K.M. Dooley, P.S. Russo, Sculpting the internal architecture of fluorescent silica particles via a template-free approach, J. Colloid Interface Sci. 467 (2016) 321–334, http://dx.doi.org/10.1016/j.jcis.2016.01.007.
[17] A. van Blaaderen, A. Vrij, Synthesis and characterization of colloidal dispersions of fluorescent, monodisperse silica spheres, Langmuir 8 (1992) 2921–2931, http://dx.doi.org/10.1021/la00048a013.
[18] P.D. Mcnaughter, J.C. Bear, P.D. Mcnaughter, J.C. Bear, D.C. Steytler, A.G. Mayes, T. Nann, A thin silica-polymer shell for functionalizing colloidal inorganic nanoparticles, Angew. Chemie Int. Ed. 50 (2011) 10384–10387, http://dx.doi.org/10.1002/anie.201103954.
[19] X. He, Y. Wang, K. Wang, M. Chen, S. Chen, Fluorescence resonance energy transfer mediated large stokes shifting near-infrared fluorescent silica nanoparticles for in vivo small-animal imaging, Anal. Chem. 84 (2012) 9056–9064, http://dx.doi.org/10.1021/ac301461s.
[20] A.M. Santiago, T. Ribeiro, A.S. Rodrigues, B. Ribeiro, R.F.M. Frade, C. Baleizão, J. Paulo, S. Farinha, Multifunctional hybrid silica nanoparticles with a fluorescent core and active targeting shell for fluorescence imaging biodiagnostic applications, Eur. J. Inorg. Chem. (2015) 4579–4587, http://dx.doi.org/10.1002/ejic.201500580.
[21] K. Vuu, J. Xie, M.A. McDonald, M. Bernardo, F. Hunter, Y. Zhang, K. Li, M. Bednarski, S. Guccione, Gadolinium-rhodamine nanoparticles for cell labeling and tracking via magnetic resonance and optical imaging, Bioconjug. Chem. 16 (2005) 995–999, http://dx.doi.org/10.1021/bc050085z.
[22] Y. Zhang, M. Hensel, Evaluation of nanoparticles as endocytic tracers in cellular microbiology, Nanoscale 5 (2013) 9296–9309, http://dx.doi.org/10.1039/C3NR01550E.
[23] L. Spötl, A. Sarti, M.P. Dierich, J. Möst, Cell membrane labeling with fluorescent dyes for the demonstration of cytokine-induced fusion between monocytes and tumor cells, Cytometry 21 (1995) 160–169, http://dx.doi.org/10.1002/cyto.990210208.
[24] Y. Ge, Y. Zhang, S. He, F. Nie, G. Teng, N. Gu, Fluorescence modified chitosan-coated magnetic nanoparticles for high-efficient cellular imaging, Nanoscale Res. Lett. 4 (2009) 287–295, http://dx.doi.org/10.1007/s11671-008-9239-9.
[25] T. Biver, N. Eltugral, A. Pucci, G. Ruggeri, A. Schena, F. Secco, M. Venturini, Synthesis, characterization, DNA interaction and potential applications of gold nanoparticles functionalized with Acridine Orange fluorophores, Dalt. Trans. 40 (2011) 4190–4199, http://dx.doi.org/10.1039/C0DT01371D.
[26] J. Gao, J. Zhong, L. Bai, J. Liu, G. Zhao, X. Sun, Revealing the role of catalysts in carbon nanotubes and nanofibers by scanning transmission X-ray microscopy, Sci. Rep. 4 (2014), http://dx.doi.org/10.1038/srep03606.

[27] I. Rivero Berti, M.L.D. Arciprete, M.L. Dittler, A. Miñan, M.F.L. de Mele, M. Gonzalez, Delivery of fluorophores by calcium phosphate-coated nanoliposomes and interaction with Staphylococcus aureus biofilms, Colloids Surfaces B Biointerfaces 142 (2016) 214–222, http://dx.doi.org/10.1016/j.colsurfb.2016.03.003.
[28] R. Sjöback, J. Nygren, M. Kubista, Absorption and fluorescence properties of fluorescein, Spectrochim. Acta Part A Mol. Biomol. Spectrosc. 51 (1995) L7–L21, http://dx.doi.org/10.1016/0584-8539(95)01421-P.
[29] J. Xu, L. Sun, J. Li, J. Liang, H. Zhang, W. Yang, FITC and Ru(phen)32+ co-doped silica particles as visualized ratiometric pH indicator, Nanoscale Res. Lett. 6 (2011) 1–7, http://dx.doi.org/10.1186/1556-276X-6-561.
[30] A. van Blaaderen, A. Vrij, Synthesis and characterization of monodisperse colloidal organo-silica spheres, J. Colloid Interface Sci. 156 (1993) 1–18, http://dx.doi.org/10.1006/jcis.1993.1073.
[31] H.-H. Yang, H.-Y. Qu, P. Lin, S.-H. Li, M.-T. Ding, J.-G. Xu, Nanometer fluorescent hybrid silica particle as ultrasensitive and photostable biological labels, Analyst 128 (2003) 462–466, http://dx.doi.org/10.1039/B210192K.
[32] I. Breßler, B.R. Pauw, A. Thünemann, McSAS: A package for extracting quantitative form-free distributions, (2014) 18.
[33] B.R. Pauw, J.S. Pedersen, S. Tardif, M. Takata, B.B. Iversen, Improvements and considerations for size distribution retrieval from small-angle scattering data by Monte Carlo methods, J. Appl. Crystallogr. 46 (2013) 365–371, http://dx.doi.org/10.1107/S0021889813001295.
[34] E. San Roman, M.C. Gonzalez, Analysis of spectrally resolved kinetic data and time-resolved spectra by bilinear regression, J. Phys. Chem. 93 (1989) 3532–3536.
[35] S. Huh, J.W. Wiench, J.-C. Yoo, M. Pruski, V.S.-Y. Lin, Organic functionalization and morphology control of mesoporous silicas via a co-condensation synthesis method, Chem. Mater. 15 (2003) 4247–4256.
[36] F. Branda, B. Silvestri, G. Luciani, A. Costantini, The effect of mixing alkoxides on the Stöber particles size, Colloids Surfaces A Physicochem. Eng. Asp. 299 (2007) 252–255, http://dx.doi.org/10.1016/j.colsurfa.2006.11.048.
[37] S. Chen, S. Hayakawa, Y. Shirosaki, E. Fujii, K. Kawabata, K. Tsuru, A. Osaka, Sol-gel synthesis and microstructure analysis of amino-modified hybrid silica nanoparticles from aminopropyltriethoxysilane and tetraethoxysilane, J. Am. Ceram. Soc. 92 (2009) 2074–2082, http://dx.doi.org/10.1111/j.1551-2916.2009.03135.x.
[38] Q. Liu, P. Deshong, M.R. Zachariah, One-step synthesis of dye-incorporated porous silica particles, J. Nanoparticle Res. 14 (2012), http://dx.doi.org/10.1007/s11051-012-0923-4.
[39] A. Calvo, P.C. Angelomé, V.M. Sánchez, D.A. Scherlis, F.J. Williams, G.J.A.A. Soler-Illia, Mesoporous aminopropyl-functionalized hybrid thin films with modulable surface and environment-responsive behavior, Chem. Mater. 20 (2008) 4661–4668.
[40] S.-W. Ha, C.E. Camalier, G.R. Beck Jr., J.-K. Lee, New method to prepare very stable and biocompatible fluorescent silica nanoparticles, Chem. Commun. (2009) 2881–2883, http://dx.doi.org/10.1039/B902195G.
[41] X. Wang, Y.-H. Tseng, J.C.C. Chan, S. Cheng, Catalytic applications of aminopropylated mesoporous silica prepared by a template-free route in flavanones synthesis, J. Catal. 233 (2005) 266–275, http://dx.doi.org/10.1016/j.jcat.2005.04.007.
[42] T.H. Lee, J.W. Rabalais, X-ray photoelectron spectra and electronic structure of some diamine compounds, J. Electron Spectros. Relat. Phenomena. 11 (1977) 123–127, http://dx.doi.org/10.1016/0368-2048(77)85052-4.
[43] S. Eiden-Assmann, B. Lindlar, G. Maret, Synthesis and characterization of colloidal fluorescent mesoporous silica particles, J. Colloid Interface Sci. 271 (2004) 120–123, http://dx.doi.org/10.1016/j.jcis.2003.11.011.
[44] Q. Hu, Development and Characterization of Fluorescent pH Sensors Based on Porous Silica and Hydrogel Support Matrices, Michigan Technological University, 2013.
[45] S. Santra, B. Liesenfeld, C. Bertolino, D. Dutta, Z. Cao, W. Tan, B.M. Moudgil, R.A. Mericle, Fluorescence lifetime measurements to determine the core–shell nanostructure of FITC-doped silica nanoparticles: an optical approach to evaluate nanoparticle photostability, J. Lumin. 117 (2006) 75–82, http://dx.doi.org/10.1016/j.jlumin.2005.04.008.
[46] H. Miyoshi, Y. Matsuo, Y. Liu, T. Sakata, H. Mori, Behavior of fluorescent molecules bound to the interior of silica nanocapsules in various solvents, J. Colloid Interface Sci. 331 (2009) 507–513, http://dx.doi.org/10.1016/j.jcis.2008.09.026.
[47] A. Imhof, M. Megens, J.J. Engelberts, D.T.N. de Lang, R. Sprik, W.L. Vos, Spectroscopy of fluorescein (FITC) dyed colloidal silica spheres, J Phys Chem B. 103 (1999), http://dx.doi.org/10.1021/jp983241q.
[48] B. Liu, S. Fletcher, M. Avadisian, P.T. Gunning, C.C. Gradinaru, A. Photostable, PH-Invariant fluorescein derivative for single-molecule microscopy, J. Fluoresc. 19 (2009) 915–920, http://dx.doi.org/10.1007/s10895-009-0492-9.
[49] S. De, R. Kundu, Spectroscopic studies with fluorescein dye – protonation, aggregation and interaction with nanoparticles, J. Photochem. Photobiol. A Chem. 223 (2011) 71–81, http://dx.doi.org/10.1016/j.jphotochem.2011.07.002.
[50] A. Auger, J. Samuel, O. Poncelet, O. Raccurt, A comparative study of non-covalent encapsulation methods for organic dyes into silica nanoparticles, Nanoscale Res. Lett. 6 (2011) 328, http://dx.doi.org/10.1186/1556-276X-6-328.
[51] L. Tarpani, L. Latterini, Effect of metal nanoparticles on the photophysical behaviour of dye-silica conjugates, Photochem. Photobiol. Sci. 13 (2014) 884–890, http://dx.doi.org/10.1039/C3PP50450F.